Elastic and viscoelastic effects in rubber/air acoustic band gap structures: A theoretical and experimental study

B. Merheb,[1,a)] P. A. Deymier,[1] M. Jain,[2] M. Aloshyna-Lesuffleur,[2] S. Mohanty,[2] A. Berker,[2] and R. W. Greger[3]
[1]*Department of Materials Science and Engineering, University of Arizona, Tucson, Arizona 85721, USA*
[2]*Corporate Research Materials Laboratory, 3M Co., 3M Center, St. Paul, Minnesota 55144-1000, USA*
[3]*Volt Services Group, Corporate Research Materials Laboratory, 3M Co., 3M Center, St. Paul, Minnesota 55144-1000, USA*

(Received 6 January 2008; accepted 24 July 2008; published online 25 September 2008)

The transmission of acoustic waves through centimeter-scale elastic and viscoelastic two-dimensional silicone rubber/air phononic crystal structures is investigated theoretically and experimentally. We introduce a finite difference time domain method for two-dimensional elastic and viscoelastic composite structures. Elastic fluid-solid phononic crystals composed of a two-dimensional array of cylindrical air inclusions in a solid rubber matrix, as well as an array of rubber cylinders in an air matrix, are shown to behave similarly to fluid-fluid composite structures. These systems exhibit very wide band gaps in their transmission spectra that extend to frequencies in the audible range of the spectrum. This effect is associated with the very low value of the transverse speed of sound in rubber compared to that of the longitudinal polarization. The difference in transmission between elastic and viscoelastic rubber/air crystals results from attenuation of transmission over a very wide frequency range, leaving only narrow passing bands at very low frequencies. These phononic crystals demonstrate the practical design of elastic or viscoelastic solid rubber/air acoustic band gap sound barriers with small dimensions. © *2008 American Institute of Physics*. [DOI: 10.1063/1.2980330]

I. INTRODUCTION

During the past decade, numerous theoretical and experimental studies have focused on the propagation of elastic waves in phononic crystals.[1–6] Phononic crystals are composed of two-dimensional (2D) or three-dimensional periodic repetitions of some inclusions inside a matrix. The matrix and inclusions can be constituted of solids or fluids. Band gaps in the band structure and in the transmission spectrum of phononic crystals form for large contrasts in the elastic coefficients and the mass densities of the matrix and inclusion materials. Acoustic band gap (ABG) structures, also called sonic crystals, are therefore phononic crystals with band gaps in the acoustic range of frequencies. Since the band gaps result from Bragg scattering of the elastic waves by the periodic array of inclusions, the lowest frequency at which a gap appears is therefore limited by the size of the periodicity of the array of inclusions. Elastic fluid/fluid ABGs have been shown to possess band gaps at significantly lower frequencies than their solid/solid and solid/fluid counterpart[2] due in part to the absence of transverse polarization.

In spite of the extensive literature on elastic phononic crystals, there is very little information concerning the properties of phononic crystals composed of viscoelastic materials. There is a theoretical demonstration of the existence of an absolute band gap in the transmission spectrum of a three-dimensional sonic crystal composed of viscoelastic spherical inclusions in air.[7] In that study the viscoelastic medium was modeled with a simple Kelvin–Voigt model.

In this present paper we consider 2D elastic and viscoelastic silicone rubber/air ABG structures. These are 2D array of cylinders of air inclusions in a solid rubber matrix as well as arrays of rubber cylinders in an air matrix. First, we investigate theoretically and experimentally the transmission properties of these ABG structures. We pay particular attention to the transmission behavior in the audible range of acoustic frequencies. Indeed the commercially available rubber studied here possesses a transverse speed of sound that is an order of magnitude, or more, smaller than the longitudinal speed of sound. The longitudinal speed of sound in rubbers is comparable to that of water and rubber/air phononic crystals are expected to show behaviors similar to that of the well-known water/air structures that possess wide band gaps at very low frequencies.[2] We show that for the particular silicone rubber studied here, an elastic representation is sufficient for understanding the experimental spectrum. However, since many polymers and rubbers exhibit viscoelastic properties, we have extended our theoretical study to include viscoelasticity. While the moduli of linear elastic materials are independent of frequency, linear viscoelastic materials have dynamic moduli that decrease with decreasing frequency. The mechanical response of viscoelastic materials will therefore vary over time, providing a dissipative mechanism that is absent in linear elastic materials. In this study, viscoelasticity is modeled with a compressible general linear viscoelastic fluid (GLVF) model. Numerical calculations of

a)Electronic mail: bassam@merheb.net.

transmission spectra are conducted by extending the finite difference time domain (FDTD) method to account for time-dependent moduli. This viscoelastic FDTD method is introduced and described in detail in Sec. II. In the results, Sec. III, we show theoretically and experimentally that the elastic rubber/air ABG structures with centimeter dimensions exhibit very wide band gaps extending to low frequencies. These gaps result from the very large contrast between the longitudinal and transverse speeds of sound in rubber. The silicone rubber-air systems, therefore, mimic the behavior of fluid/fluid systems. Moreover we show theoretically that the transmission properties of linear viscoelastic ABG materials differ significantly from the behavior of linear elastic materials. Viscoelasticity impacts the transmission spectrum by attenuating transmission within the passing bands of the structure. The conclusions drawn from this joint experimental and theoretical study are reported in Sec. IV.

II. METHODS AND MODELS

In the present study, we conduct FDTD calculations of transmission spectra of elastic rubber-air phononic crystals. The FDTD method for elastic composite media is well documented[8] and not described in this paper; however, we also consider here theoretically the effect of the viscoelasticity on the transmission spectrum of phononic crystals. For this purpose we develop in detail in this section an efficient FDTD method that accounts for viscoelasticity within a Maxwell–Weichert model. We finally, describe the experimental method employed to measure transmission spectra of rubber/air ABG structures.

A. Computational method

The elastic wave equation is given by

$$\frac{\partial \mathbf{v}}{\partial t} = \frac{1}{\rho}\text{div}\ \sigma, \tag{1}$$

where t is the time, ρ is the mass density, $\mathbf{v}(t)$ is the velocity vector, and σ is the total stress tensor.

To calculate the stress tensor we employ the constitutive equation for the GLVFs. The compressible generalized linear viscoelastic solid relation is properly invariant and obeys the principle of material objectivity. Furthermore, while there are a myriad number of alternative, properly invariant, constitutive relations to choose from for nonlinear viscoelasticity, all of these must reduce to the generalized linear viscoelastic material model in the linear viscoelastic limit. Since we are primarily interested in linear acoustics that involve small strains, one is justified in restricting the material's rheological behavior to be linear as well, in which case the only properly invariant constitutive relation that one is justified to use is the generalized linear viscoelastic model.

When the GLVF material is compressible, the total stress tensor is given by

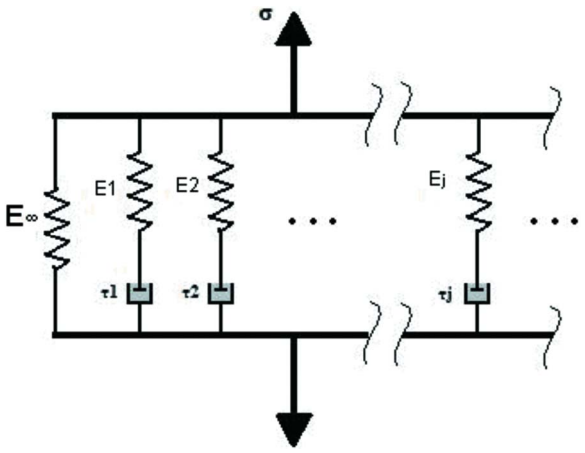

FIG. 1. (Color online) Spring and dashpot illustrations of the Maxwell–Weichert model.

$$\boldsymbol{\sigma}(t) = 2\int_{-\infty}^{t} G(t-t')\mathbf{D}(t')dt' + \int_{-\infty}^{t}\left[K(t-t') - \frac{2}{3}G(t - t')\right][\nabla\cdot\mathbf{v}(t')]\mathbf{I}dt', \tag{2}$$

where $\mathbf{D}(\mathbf{x},t)$ is the rate of deformation tensor given by

$$\mathbf{D} = \tfrac{1}{2}[(\nabla\mathbf{v}) + (\nabla\mathbf{v})^T] \tag{3}$$

and $G(t)$ and $K(t)$ are the steady shear and bulk moduli, respectively. These moduli can be experimentally determined through rheometry and the data can be fitted in a variety of ways, including the use of mechanical-analog models. A viscoelastic model or in effect the behavior pattern it describes may be illustrated schematically by combinations of springs and dashpots, representing elastic and viscous factors, respectively. Hence, a spring is assumed to reflect the properties of an elastic deformation, and similarly a dashpot is assumed to depict the characteristics of viscous flow. The generalized Maxwell, also known as the Maxwell–Weichert, model takes into account the fact that the relaxation does not occur with a single time constant but with a distribution of relaxation times. The Weichert model shows this by having as many spring-dashpot Maxwell elements as are necessary to accurately represent the distribution (Fig. 1). A multiple element Maxwell model is therefore more apt to represent the numerous time scales associated with relaxation in real viscoelastic materials.

For an n-element generalized Maxwell solid model the extensional modulus $E(t)$ is calculated to be

$$E(t) = E_\infty + \sum_{i=1}^{n} E_i e^{-t/\tau_i}, \tag{4}$$

where $\{E_i,\tau_i;i=1,2,\ldots,n\}$ are the moduli and relaxation times of the elements and $E_\infty = E(\infty)$ is the equilibrium extensional modulus. We use the generalized Maxwell form for $E(t)$ only as a convenient fit to our modulus data that we obtained by performing dynamic mechanical analysis (DMA) tests in extensional mode on a sample of a commercial silicone elastomer.

By introducing $\alpha(t)$ as a function having the same form as $E(t)$:

$$\alpha(t) = \alpha_0 + \sum_{i=1}^{n} \alpha_i e^{-t/\tau_i}, \tag{5}$$

where

$$\alpha_0 = \frac{E_\infty}{E_{\text{sum}}}, \quad \alpha_i = \frac{E_i}{E_{\text{sum}}} \quad (i = 1,2,\ldots,n)$$

and

$$\sum_{i=0}^{n} \alpha_i = 1, \quad E_{\text{sum}} = \sum_{i=1}^{n} E_i,$$

we obtain

$$E(t) = E_{\text{sum}}\alpha(t). \tag{6}$$

Consequently, we assume that

$$E(t) = 2G(t)(1+\upsilon) = 3K(t)(1-2\upsilon), \tag{7}$$

with

$$G(t) = G_{\text{sum}}\alpha(t),$$

$$K(t) = K_{\text{sum}}\alpha(t) \tag{8}$$

and

$$G_{\text{sum}} = \mu,$$

$$K_{\text{sum}} - \frac{2}{3}G_{\text{sum}} = \lambda. \tag{9}$$

In Eqs. (7) and (9), ν is Poisson's ratio and λ and μ are the Lamé constant and shear modulus, respectively.

Now we consider a 2D elastic/viscoelastic material, where the system is infinite in the vertical direction z, and none of its properties depends on z (translational invariance). In this case the Cartesian components of the 2D stress tensor become

$$\sigma_{xx}(t) = 2\int_{-\infty}^{t} G(t-t')\frac{\partial v_x}{\partial x}(t')dt' + \int_{-\infty}^{t}\left(K(t-t') - \frac{2}{3}G(t-t')\right)\left(\frac{\partial v_x}{\partial x}(t') + \frac{\partial v_y}{\partial y}(t')\right)dt', \tag{10}$$

$$\sigma_{yy}(t) = 2\int_{-\infty}^{t} G(t-t')\frac{\partial v_y}{\partial y}(t')dt' + \int_{-\infty}^{t}\left(K(t-t') - \frac{2}{3}G(t-t')\right)\left(\frac{\partial v_x}{\partial x}(t') + \frac{\partial v_y}{\partial y}(t')\right)dt', \tag{11}$$

$$\sigma_{xy}(t) = \sigma_{yx}(t) = \int_{-\infty}^{t} G(t-t')\left(\frac{\partial v_x}{\partial y}(t') + \frac{\partial v_y}{\partial x}(t')\right)dt'. \tag{12}$$

For the sake of illustration, let us insert Eq. (8) into Eq. (10). Using $C_{11}=2\mu+\lambda$, $C_{12}=\lambda$, and $C_{44}=\mu$, $\sigma_{xx}(t)$ become

$$\sigma_{xx}(t) = \alpha_0 C_{11}\frac{\partial u_x}{\partial x}(t) + \alpha_0 C_{12}\frac{\partial u_y}{\partial y}(t) + C_{11}\sum_{1}^{n}\alpha_i\int_{-\infty}^{t}\frac{\partial v_x}{\partial x}(t')e^{-(t-t')/\tau_i}dt' + C_{12}\sum_{1}^{n}\alpha_i\int_{-\infty}^{t}\frac{\partial v_y}{\partial y}(t')e^{-(t-t')/\tau_i}dt'. \tag{13}$$

The elastic behavior is recovered by setting $\alpha_0=1$ and $\alpha_i=0$ for $i=1,\ldots,n$ ($E_\infty>0$ and $E_i=0$ for $i=1,\ldots,n$).

The difficulty of the problem consists in the calculation of integrals of the type

$$Ixx_i(t) = \int_{-\infty}^{t}\frac{\partial v_x(t')}{\partial x}e^{-(t-t')/\tau_i}dt'. \tag{14}$$

We show in the Appendix that $Ixx_i(t)$ can be calculated by a recursive method:

$$Ixx_i(t+dt) = \left[\frac{\frac{\partial v_x(t)}{\partial x}e^{-dt/\tau_i} + \frac{\partial v_x(t+dt)}{\partial x}}{2}\right]dt + e^{-dt/\tau_i}Ixx_i(t), \tag{15}$$

where $Ixx_i(0)=0$.

Similar equations are obtained for the yy and xy components (see the Appendix).

We can now develop the FDTD method for the generalized Maxwell model. This involves transforming the governing differential equations in the time domain into finite differences and solving them as one progresses in time in small increments. These equations comprise the basis for the implementation of the FDTD in 2D viscoelastic systems. For the implementation of the FDTD method we divide the computational domain into $N_x \times N_y$ subdomains (grids) with dimension dx, dy. For space derivatives we use central differences, where the y direction is staggered to the x direction. For the time derivative we use forward difference, with a time interval dt.

Using expansions at point (i,j) and time (n), Eq. (1) in component form becomes

$$v_x^{n+1}(i,j) = v_x^n(i,j) + \frac{dt}{\rho(i,j)}\left(\frac{\sigma_{xx}^{n+1}(i,j) - \sigma_{xx}^{n+1}(i-1,j)}{dx} + \frac{\sigma_{xy}^{n+1}(i,j) - \sigma_{xy}^{n+1}(i,j-1)}{dy}\right), \tag{16}$$

$$v_y^{n+1}(i,j) = v_y^n(i,j) + \frac{dt}{\rho(i+1/2,j+1/2)}\left(\frac{\sigma_{yy}^{n+1}(i,j+1) - \sigma_{xx}^{n+1}(i,j)}{dy} + \frac{\sigma_{xy}^{n+1}(i+1,j) - \sigma_{xy}^{n+1}(i,j)}{dx}\right), \tag{17}$$

where

$$\rho(i+1/2,j+1/2) = \sqrt[4]{\rho(i,j)\rho(i+1,j)\rho(i,j+1)\rho(i+1,j+1)}.$$

The stress component σ_{xx} is calculated by discretizing Eq. (13), using expansion at point (i,j) and time (n), and including the recursive form of the integral from Eq. (15):

$$\sigma_{xx}^{n+1}(i,j) = \alpha_0(i+1/2,j)C_{11}(i + 1/2,j)\frac{u_x^n(i+1,j)-u_x^n(i,j)}{dx} + \alpha_0(i + 1/2,j)C_{12}(i+1/2,j)\frac{u_y^n(i,j)-u_y^n(i,j-1)}{dy} + C_{11}(i+1/2,j)\sum_{p=1}^{n}\alpha_p(i+1/2,j) \times\left[\frac{v_x^n(i+1,j)-v_x^n(i,j)}{2dx} + \frac{v_x^{n-1}(i+1,j)-v_x^{n-1}(i,j)}{2dx}e^{-dt/\tau_p(i+1/2,j)} + e^{-dt/\tau_p(i,j)}I_{xx_p}^n\right] + C_{12}(i+1/2,j)\sum_{p=1}^{n}\alpha_p(i + 1/2,j)\left[\frac{v_y^n(i,j)-v_y^n(i,j-1)}{2dy} + \frac{v_y^{n-1}(i,j)-v_y^{n-1}(i,j-1)}{2dy}e^{-dt/\tau_p(i+1/2,j)} + e^{-dt/\tau_p(i,j)}I_{yy_p}^n\right]. \quad (18)$$

We define

$$C_{11}(i+1/2,j) = \sqrt{C_{11}(i+1,j)C_{11}(i,j)},$$

$$C_{12}(i+1/2,j) = \sqrt{C_{12}(i+1,j)C_{12}(i,j)},$$

and

$$\alpha_p(i+1/2,j) = \sqrt{\alpha_p(i+1,j)\alpha_p(i,j)}, \quad p = 0,1,2,\ldots,n.$$

Similarly, the components σ_{yy} and σ_{xy} are obtained in discretized form:

$$\sigma_{yy}^{n+1}(i,j) = \alpha_0(i+1/2,j)C_{11}(i + 1/2,j)\frac{u_y^n(i,j)-u_y^n(i,j-1)}{dy} + \alpha_0(i + 1/2,j)C_{12}(i+1/2,j)\frac{u_x^n(i+1,j)-u_x^n(i,j)}{dx} + C_{11}(i+1/2,j)\sum_{p=1}^{n}\alpha_p(i+1/2,j) \times\left[\frac{v_y^n(i,j)-v_y^n(i,j-1)}{2dy} + \frac{v_y^{n-1}(i,j)-v_y^{n-1}(i,j-1)}{2dy}e^{-dt/\tau_p(i+1/2,j)} + e^{-dt/\tau_p(i,j)}I_{yy_p}^n\right] + C_{12}(i+1/2,j)\sum_{p=1}^{n}\alpha_p(i + 1/2,j)\left[\frac{v_x^n(i+1,j)-v_x^n(i,j)}{2dx} + \frac{v_x^{n-1}(i+1,j)-v_x^{n-1}(i,j)}{2dx}e^{-dt/\tau_p(i+1/2,j)} + e^{-dt/\tau_p(i,j)}I_{xx_p}^n\right], \quad (19)$$

$$\sigma_{xy}^{n+1}(i,j) = \alpha_0(i,j+1/2)C_{44}(i,j+1/2) \times\left[\frac{u_x^n(i,j+1)-u_x^n(i,j)}{dy} + \frac{u_y^n(i,j)-u_y^n(i-1,j)}{dx}\right] + C_{44}(i,j + 1/2)\sum_{p=1}^{n}\alpha_p(i,j+1/2)\left[\frac{v_x^n(i,j+1)-v_x^n(i,j)}{2dy} + \frac{v_x^{n-1}(i,j+1)-v_x^{n-1}(i,j)}{2dy}e^{-dt/\tau_p(i,j+1/2)} + e^{-dt/\tau_p(i,j)}I_{xy_p}^n\right] + C_{44}(i,j+1/2)\sum_{p=1}^{n}\alpha_p(i,j + 1/2)\left[\frac{v_y^n(i,j)-v_y^n(i-1,j)}{2dx} + \frac{v_y^{n-1}(i,j)-v_y^{n-1}(i-1,j)}{2dx}e^{-dt/\tau_p(i,j+1/2)} + e^{-dt/\tau_p(i,j)}I_{yx_p}^n\right], \quad (20)$$

where

$$C_{44}(i,j+1/2) = \sqrt{C_{44}(i,j+1)C_{44}(i,j)},$$

$$\alpha_p(i,j+1/2) = \sqrt{\alpha_p(i,j+1)\alpha_p(i,j)}, \quad p = 0,1,2,\ldots,n.$$

It has to be mentioned that the above way of discretizing the equations ensures second order accurate central difference for the space derivatives. The field components u_x and u_y have to be centered in different space points.

The FDTD method for elastic and viscoelastic media is local in space and ideally suited for computer simulation on parallel platforms. All the calculations reported are performed on at least eight parallel processors.

B. Model structures

We study two model structures illustrated in Figs. 2 and 3. These structures are composed of three separate regions. The central region is a phononic crystal modeled as arrays of cylindrical inclusions with circular cross section made of isotropic material, embedded in an isotropic material matrix. The cylinders, with diameter d, are assumed to be parallel to the Z axis of the Cartesian coordinates $(OXYZ)$. The array is

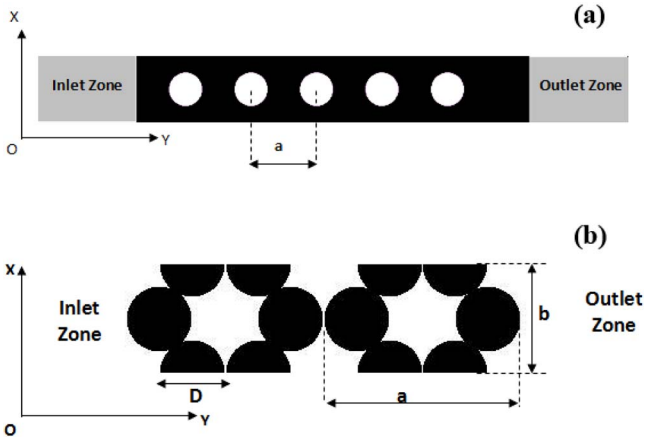

FIG. 2. (Color online) (a) 2D cross section of the FDTD model structure with a square array of air cylinders embedded in a rubber matrix, lattice parameter $a=12$ mm, and cylinder diameter $D=8$ mm. (b) 2D cross section of the model structure with an array of rubber cylinders located on a honeycomb lattice embedded in air, vertical lattice parameter $b=19.9$ mm, horizontal lattice parameter $a=34.5$ mm, and cylinder diameter $D=11.5$ mm. In both cases the cylinders are parallel to the Z axis of the Cartesian coordinate system $(OXYZ)$.

then considered infinite in the two directions X and Z and finite in the direction of propagation of the probing wave (Y). The periodicity along the direction X is ensured by the application of periodic boundary conditions. In Fig. 2(a) the matrix is made of rubber and the inclusions are made of air. In Fig. 2(b) the matrix is air and the cylinders are composed of rubber. For all calculations reported here, the physical characteristics of the rubber are those of a polysilicone rubber with mass density=1260 kg/m^3, longitudinal speed =1200 m/s, and transverse speed=20 m/s.[9] The longitudinal speed of sound was measured in our laboratory by a time of flight method (see Sec. II C). We have not been able to measure reliably the transverse speed of sound; however, we estimate it to be ~20 m/s from published data on physical constants with different rubbers.[9] Air is modeled as a fluid with mass density=1.3 kg/m^3 and longitudinal speed =340 m/s. In Fig. 2(a) the air cylinders have a diameter of 8 mm and are arranged on a 6×1 square array with a lattice parameter $a=12$ mm. The second structure represented in Fig. 2(b) consists of an array of touching polymer cylinders located on a honeycomb lattice with a hexagon edge size of 11.5 mm and cylinder radius of 5.75 mm.

For the calculations including the effect of viscoelasticity, we use the experimental values (E_i, τ_i) of the extensional modulus $E(t)$, which is obtained by performing DMA tests in extensional mode on a sample of a commercial silicone elastomer to obtain α_i $(i=0,\ldots,8)$ according to Eq. (5) for an eight-element Maxwell model. The different values for E_i, τ_i, and α_i are presented in Table I.

The phononic crystal region is sandwiched between two homogeneous regions subsequently called the inlet and outlet regions. These regions are elastic media with the same density and speed of sound as the matrix materials of the phononic crystal region. In the case of Fig. 2(a), the elastic inlet and outlet regions are obtained by setting $\alpha_0=1$ and $\alpha_i=0$ for $i=1,\ldots,n$. We use elastic inlet and outlet regions in order to apply the Mur absorbing boundary conditions[8] at

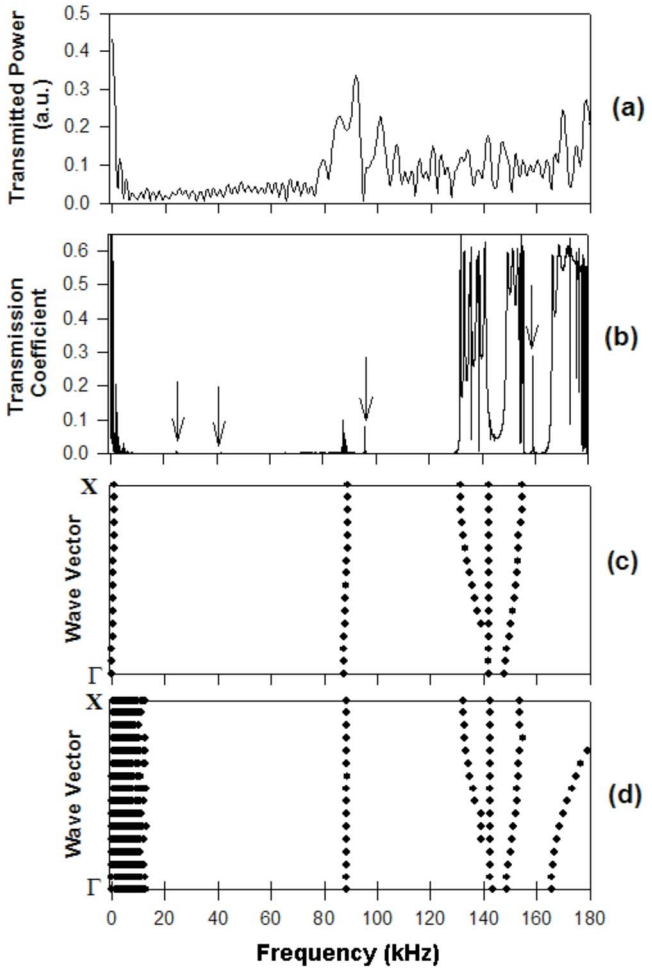

FIG. 3. (Color online) Transmission spectra and band structures of the rubber matrix air inclusion system: (a) experimentally measured transmitted power (in arbitrary units) vs frequency for the 6×6 air inclusions/silicon rubber sample. (b) Calculated transmission coefficient for longitudinal waves considering the rubber as an elastic medium. (c) Band structure along the Γ-X direction of the first Brillouin zone, approximating the rubber as a fluidlike medium ($c_t=0$ m/s). The wave vector is parallel to an edge of the square lattice and varies in the interval $[0-\pi/a]$. (d) Band structure for the solid rubber ($c_t=20$ m/s).

the extreme ends of these regions. Note that in the case of a phononic crystal with a viscoelastic matrix, the interface between the elastic inlet and outlet regions and the viscoelastic matrix will lead to some reflections of acoustic waves. The width of the inlet and outlet regions is 20 mm.

TABLE I. Values of the viscoelastic parameters α_i and τ_i used in the FDTD calculations.

Relaxation time τ_i (s)	E_i (dyn/cm^2)	α_i
	2.13×10^7	0.08
4.32×10^{-9}	9.00×10^7	0.36
5.84×10^{-8}	4.20×10^7	0.17
3.51×10^{-7}	2.94×10^7	0.12
2.28×10^{-6}	2.41×10^7	0.10
1.68×10^{-5}	1.87×10^7	0.08
2.82×10^{-4}	1.31×10^7	0.05
7.96×10^{-3}	7.02×10^6	0.03
9.50×10^{-3}	4.45×10^6	0.02

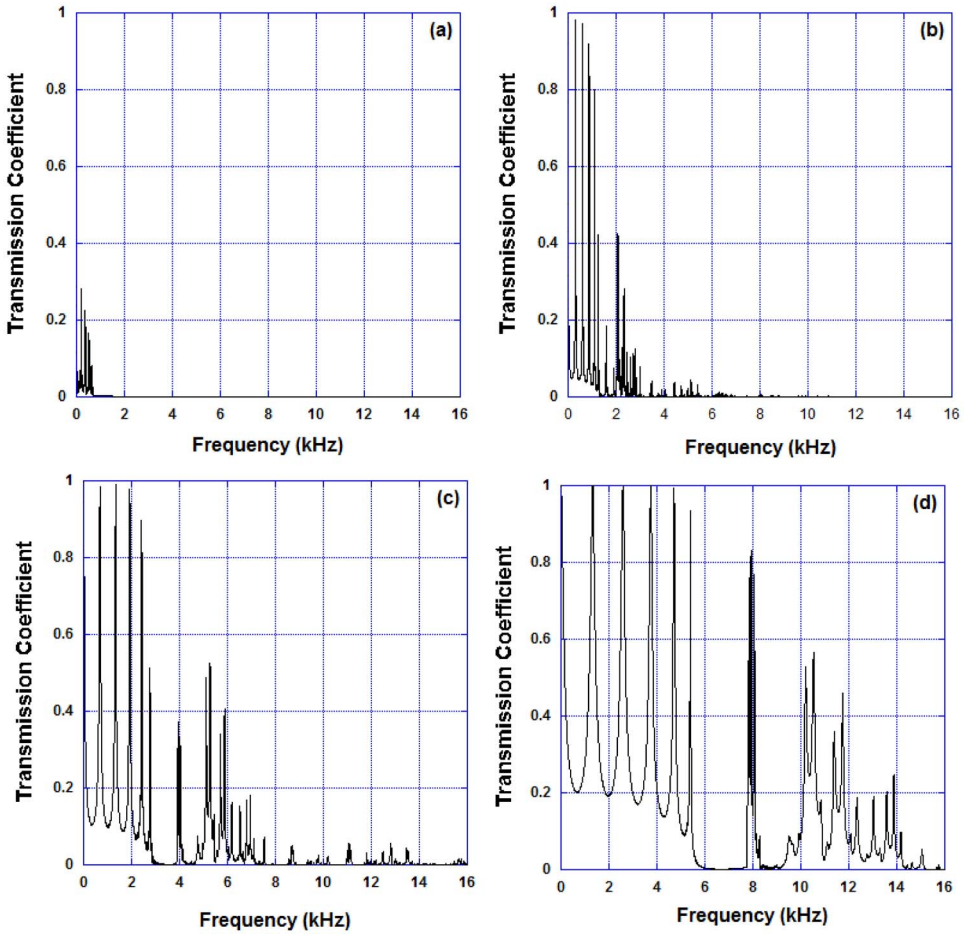

FIG. 4. (Color online) Low frequency transmission coefficient for different values of the transverse wave speed of sound for the elastic rubber-air composite: (a) $c_t=0$ m/s, (b) $c_t=20$ m/s, (c) $c_t=50$ m/s, and (d) $c_t=100$ m/s.

A stimulus sound wave packet taking the form of a Gaussian-modulated cosine waveform is launched in the inlet region. The displacement amplitude of the stimulus is 10^{-6} m. This wave packet corresponds to a broadband signal with a chosen central frequency of 350 kHz, enabling the study of the transmission of phononic crystals from audible to ultrasonic frequencies. All the calculations reported in this paper are for $dx=dy=10^{-4}$ m or less. For calculations with purely elastic constituents, the time step dt is chosen to satisfy the Courant stability criterion. This condition is not sufficient for the calculations with viscoelastic media using our recursive method. In this case we investigated the stability of the algorithm and found that stability is achieved for time steps significantly smaller than the Courant criterion. For the calculations with viscoelasticity we therefore use a time integration step of 1.6 ns. The total simulation time for the calculation of the transmission spectra is chosen to exceed 0.01 s, which is sufficient to obtain reliable transmission coefficients.

C. Experimental method

We limit the experimental study on a sample of binary composite materials constituted of a square array of 36 (6×6) parallel cylinders of air embedded in a polymer matrix. The polymer is a silicone rubber (Dow Corning® HS II RTV high strength mold[10]). The lattice parameter is 12 mm and the diameter of the cylinder is 8 mm. The physical dimensions of the sample are $8\times8\times8$ cm^3. Experimental measurements were carried out to obtain the transmission spectrum of this sample.

The ultrasonic emission source used in the experiment is a Panametrics delta broadband 500 kHz *P* transducer with a Panametrics pulser/receiver model 500PR. The acquisition of the signal is done with a transducer identical to the source transducer connected to a Tektronix TDS 540 oscilloscope equipped with a general purpose interface bus (GPIB) data acquisition card. The cylindrical transducers (with a diameter of 3.175 cm) are centered on the face of the sample. The emission source produces compression waves (*P* waves) and the receiving transducer detects only the longitudinal component of the transmitted wave. The longitudinal speed of sound is measured by the standard method of time delay between the pulse sent and the signal received. The transmission spectrum is obtained by Fourier transforming the time evolution of the received signal

III. RESULTS

A. Rubber matrix/air inclusions structure

1. Elastic effect

In Figs. 3(a) and 3(b) we report on the experimental measurement of the transmission through the square array of air cylinders in the rubber matrix as well as the calculated transmission coefficient of the same system considering the rubber as an elastic medium. The transmission coefficient is

calculated as the ratio of the spectral power transmitted in the composite to that transmitted in an elastic homogeneous medium composed of the matrix material. In addition, Figs. 3(c) and 3(d) report on the band structure of the rubber matrix air inclusion system for wave vectors parallel to an edge of the square lattice within the first Brillouin zone $[0-\pi/a]$ for a fluidlike rubber (c) with $c_t=0$ m/s and the actual solid rubber (d) with $c_t=20$ m/s. The band structures were calculated with the FDTD method.[11]

We notice on the spectrum of Fig. 3(b) two band gaps. The most important one is from around 3 to 87 kHz; the second gap is from 90 to 125 kHz. We note also in the spectrum of Fig. 3(b) that the transmission spectrum possesses sharp narrow peaks (indicated by arrows) at well defined frequencies. These transmission peaks result from hybridization of the composite bands with flat bands corresponding to the modes of vibration of cylinders of air. The frequencies at which these flat bands occur can be obtained from the zeros of the first derivative of the Bessel function of the first kind, $J'_m(\omega r/c)=0$ where c is the speed of sound in air, r is the radius of the air cylinder, and m is the order of the Bessel function.

The experimental transmission spectrum in Fig. 3(a) exhibits a frequency region with a very low transmission between a few thousand hertz and a little less than 80 kHz. There is also a transmission band centered around 90 kHz. These two features are in excellent agreement with the calculated spectrum. Figure 3(a) does not show, for unknown reasons, the second calculated gap as transmission does not drop significantly for frequencies above 95 kHz. However, the comparison between the experimental and calculated transmission spectra below 95 kHz suggests that an elastic representation is sufficient to account for the behavior of the phononic crystal. The band structure of the solid rubber [Fig. 3(d)] is in excellent agreement with the FDTD transmission spectrum (note that we have not represented in that figure the air cylinders' flat bands). These band structures possess a large number of overlapping bands between 0 and approximately 15 kHz. A comparison of this band structure with that of a fluidlike rubber [Fig. 3(c)] indicates that the multiple bands at low frequencies are associated with transverse modes. These modes result from multiple folding of the low speed of sound transverse band of homogeneous rubber due to the periodicity of the phononic crystal. In contrast, the band structure of the fluidlike rubber possesses only one longitudinal band at very low frequencies in the interval [0–800 Hz]. Therefore, the transmission at low frequencies, in Fig. 3(b), results from the longitudinal as well as the transverse bands of Fig. 3(d).

To further elucidate the elastic behavior of the rubber-air system at low frequencies, we have calculated the transmission spectra for different values of the transverse speed of sound. The fluidlike transmission spectrum of Fig. 4(a) shows the longitudinal passing band of that system below 1 kHz. As one increases the transverse speed of sound of the solid rubber [Figs. 4(b)–4(d)], the low frequency transmission bands extend toward higher frequencies. The transmission spectra are isomorphic with frequencies scaling with the value of the transverse speed of sound. In Fig. 5, we compare

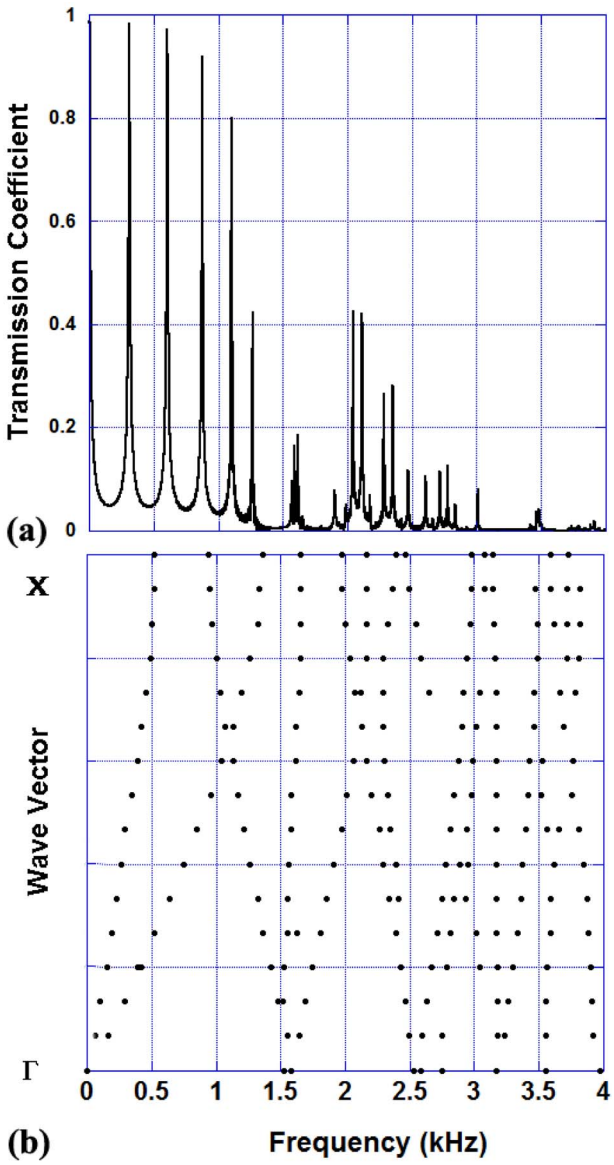

FIG. 5. (Color online) (a) Low frequency transmission coefficient for rubber matrix with $c_t=20$ m/s and the corresponding (b) band structure.

the low frequency transmission spectrum for $c_t=20$ m/s and the calculated band structure. While all the bands in the band structure cross, the transmission spectrum possesses a narrow passing band centered on a gap extending between 1.2 and 1.8 kHz. This observation indicates that the third and fifth bands from the bottom of the band structure are deaf bands with symmetry incompatible with the longitudinal nature of the simulating incident wave packet. These two bands, for instance, could only be stimulated by transverse modes.

2. Viscoelastic effects

In Fig. 6, we compare the transmission amplitude spectra in a homogeneous elastic rubber, a homogeneous hypothetical viscoelastic rubber, and a viscoelastic rubber-air composite structure with the same width and elastic properties. Attenuation by the viscoelastic rubber of the wave packet compared to the transmission in the elastic rubber is clearly seen in Fig. 6. The viscoelastic rubber-air inclusion system

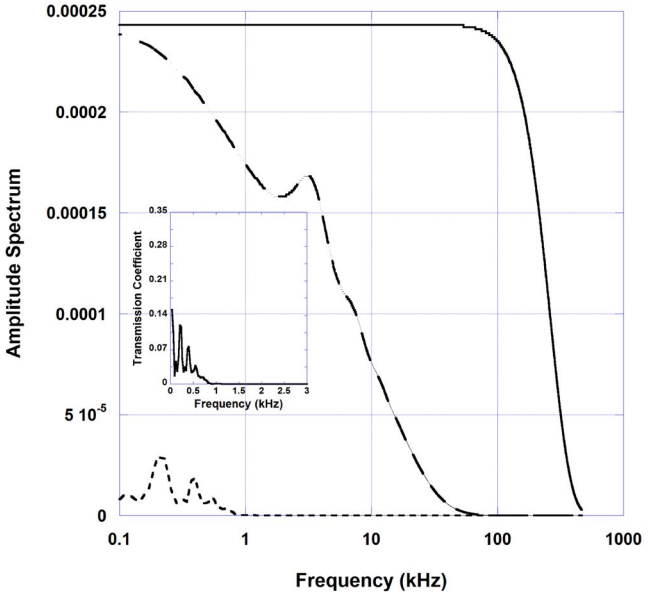

FIG. 6. (Color online) Calculated longitudinal amplitude transmitted (in arbitrary units) through a homogeneous rubber treated as an elastic medium (continuous curve), a viscoelastic medium (long dash curve), and the viscoelastic rubber matrix/air inclusion system (short dash). The probing wave packet is the same for the three systems. The inset graph reports the transmission coefficient of the viscoelastic rubber-air composite.

presents an attenuated passing band below 1 kHz. Beyond that frequency, transmission is nearly totally inexistent. We recall that the transmission in the elastic phononic crystal at low frequencies extended up to approximately 8 kHz. The transmission of the viscoelastic system at low frequencies (inset of Fig. 6) does not exceed 15% of the transmission coefficient of the elastic system [Fig. 4(b)].

B. Transmission in air /rubber structure

The calculations discussed in this section were carried out for the arrays of polymer cylinders located on a honeycomb lattice embedded in air [Fig. 2(b)]. The transmission coefficient of this structure shown in Fig. 7(a) was computed using the FDTD method for very long time integration (0.06 s). We notice a large band gap starting at 1.5 and up to more than 100 kHz. Another gap exists between 0.48 and 1.3 kHz. The transmission level for the band between 1.3 and 1.5 kHz is low (3%).

The same simulation was carried out for an air/viscoelastic rubber structure based on the generalized eight-element Maxwell model. A comparison between Figs. 7(a) and 7(b) shows a significant drop in the amplitude of the first transmitted band (<500 Hz) due to attenuation. In addition, we notice that the narrow passing band for elastic system centered on 1.2 kHz disappears or is highly attenuated by the viscoelasticity of the material.

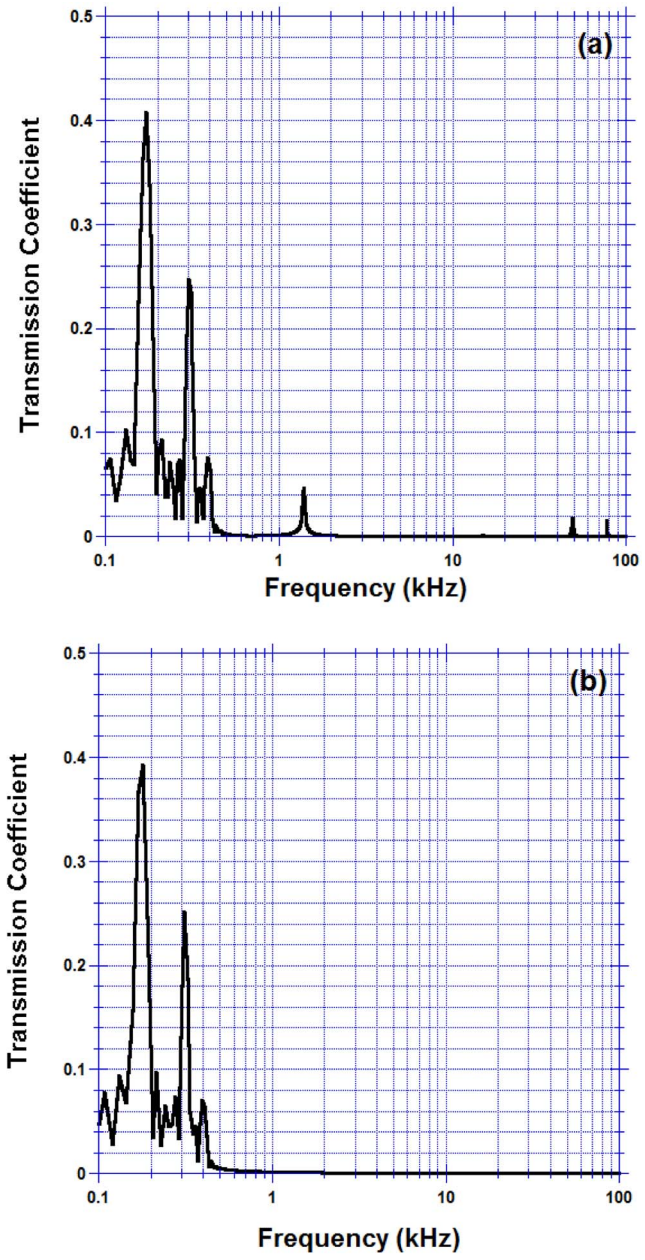

FIG. 7. (Color online) Transmission coefficient for an array of touching polymer cylinders located on a honeycomb lattice in air (cylinder radius of 5.75 mm, hexagon lattice parameter of 19.9 mm) for an (a) elastic rubber and (b) a generalized eight-element Maxwell model of the rubber. The overall thickness of the phononic crystal is 69 mm.

IV. CONCLUSION

In this study, we investigated rubber/air phononic crystals with particular attention paid to the fact that in rubber the transverse speed of sound is significantly lower than the longitudinal one and that rubbers are materials that may exhibit viscoelastic responses. Consequently, we develop a FDTD method for 2D elastic and viscoelastic composite structures. Experimental and calculated transmission spectra for an elastic rubber matrix/air inclusions phononic crystal show that the system behaves as a fluid/fluid composite due to the large contrast between the transverse and longitudinal speeds of sound. We also demonstrate that viscoelasticity can attenuate transmission over very wide ranges of frequency, leaving only passing bands at very low frequencies. The two types of structures studied here demonstrate the practical design of elastic or viscoelastic solid rubber/air ABG sound barrier with dimensions in the range of millimeters to centimeters.

APPENDIX: FDTD RECURSIVE METHOD

In this paragraph we demonstrate how to calculate the integral $Ixx_i(t)=\int_{-\infty}^{t}[\partial v_x(t')/\partial x]e^{-(t-t')/\tau_i}dt'$ by a recursive method. First we assume that for an incident wave that arrives from an elastic medium we have $\int_{-\infty}^{t}\approx\int_{0}^{t}$. Then let us denote $w=t-t'\Rightarrow dw=-dt'$. By replacing t' in the equation we obtain

$$Ixx_i(t)=\int_0^t \frac{\partial v_x(t-w)}{\partial x}e^{-w/\tau_i}dw. \tag{A1}$$

Now we calculate $Ixx_i(t+dt)$,

$$Ixx_i(t+dt)=\int_0^{t+dt} \frac{\partial v_x(t+dt-w)}{\partial x}e^{-w/\tau_i}dw, \tag{A2}$$

$$Ixx_i(t+dt)=\int_0^{dt} \frac{\partial v_x(t+dt-w)}{\partial x}e^{-w/\tau_i}dw + \int_{dt}^{t+dt} \frac{\partial v_x(t+dt-w)}{\partial x}e^{-w/\tau_i}dw. \tag{A3}$$

By changing $s=w-dt\Rightarrow ds=dw$,

$$Ixx_i(t+dt)=\int_{-dt}^{0} \frac{\partial v_x(t-s)}{\partial x}e^{-(s+dt)/\tau_i}ds + \int_0^t \frac{\partial v_x(t-s)}{\partial x}e^{-(s+dt)/\tau_i}ds, \tag{A4}$$

$$Ixx_i(t+dt)=\left[\frac{\frac{\partial v_x(t)}{\partial x}e^{-dt/\tau_i}+\frac{\partial v_x(t+dt)}{\partial x}}{2}dt\right] + e^{-dt/\tau_i}\int_0^t \frac{\partial v_x(t-s)}{\partial x}e^{-s/\tau_i}ds. \tag{A5}$$

Finally we obtain a recursive form for the integral calculation:

$$Ixx_i(t+dt)=\left[\frac{\frac{\partial v_x(t)}{\partial x}e^{-dt/\tau_i}+\frac{\partial v_x(t+dt)}{\partial x}}{2}dt\right] + e^{-dt/\tau_i}Ixx_i(t), \tag{A6}$$

where $Ixx_i(0)=0$.

Similar equations are obtained for the yy and xy components,

$$Iyy_i(t+dt)=\left[\frac{\frac{\partial v_y(t)}{\partial y}e^{-dt/\tau_i}+\frac{\partial v_y(t+dt)}{\partial y}}{2}dt\right] + e^{-dt/\tau_i}Iyy_i(t), \tag{A7}$$

$$Ixy_i(t+dt)=\left[\frac{\frac{\partial v_x(t)}{\partial y}e^{-dt/\tau_i}+\frac{\partial v_x(t+dt)}{\partial y}}{2}dt\right] + e^{-dt/\tau_i}Ixy_i(t), \tag{A8}$$

$$Iyx_i(t+dt)=\left[\frac{\frac{\partial v_y(t)}{\partial x}e^{-dt/\tau_i}+\frac{\partial v_y(t+dt)}{\partial x}}{2}dt\right] + e^{-dt/\tau_i}Iyx_i(t). \tag{A9}$$

[1] J. O. Vasseur, P. A. Deymier, A. Khelif, Ph. Lambin, B. Dajfari-Rouhani, A. Akjouj, L. Dobrzynski, N. Fettouhi, and J. Zemmouri, Phys. Rev. E **65**, 056608 (2002).
[2] Ph. Lambin, A. Khelif, J. O. Vasseur, L. Dobrzynski, and B. Djafari-Rouhani, Phys. Rev. E **63**, 066605 (2001).
[3] J. O. Vasseur, P. A. Deymier, G. Frantziskonis, G. Hong, B. Dajfari-Rouhani, and L. Dobrzynski, J. Phys.: Condens. Matter **10**, 6051 (1998).
[4] M. Sigalas, M. S. Kushwaha, E. N. Economou, M. Kafesaki, I. E. Psarobas, and W. Steurer, Z. Kristallogr. **220**, 765 (2005).
[5] M. Sigalas and E. N. Economou, Solid State Commun. **86**, 141 (1993).
[6] Z. Liu, X. Zhang, Y. Mao, Y. Y. Zhu, Z. Yang, C. T. Chan, and P. Sheng, Science **289**, 1734 (2000).
[7] I. E. Psarobas, Phys. Rev. B **64**, 012303 (2001).
[8] M. Kafesaki, M. M. Sigalas, and N. Garcia, in *Photonic Crystals and Light Localization in the 21st Century*, edited by C. M. Soukoulis (Kluwer, Dordrecht, 2001), p. 69.
[9] *Polymer Handbook*, 3rd ed., edited by J. Brandup and E. H. Immergut (Wiley, New York, 1989).
[10] Two-part silicon system, Dow Corning HSII RTV (http://www.ellsworth.com/display/productdetail.html?productid=425&Tab=Vendors).
[11] Y. Tanaka, Y. Tomoyasu, and S. Tamura, Phys. Rev. B **62**, 7387 (2000).